

Additional stratospheric NO_x production by relativistic electron precipitation during the 2004 spring NO_x descent event

Mark A. Clilverd,¹ Annika Seppälä,^{2,3} Craig J. Rodger,⁴ Martin G. Mlynczak,⁵ and Janet U. Kozyra⁶

Received 10 June 2008; revised 12 January 2009; accepted 28 January 2009; published 3 April 2009.

[1] We analyze in detail the February 2004 Global Ozone Monitoring by Occultation of Stars (GOMOS) NO₂ observations in the northern polar latitudes during the springtime descent of NO_x from the mesosphere into the stratosphere. We combine GOMOS observations with SABER-observed NO 5.3 μm radiated power and an AARDDVARK-derived radio wave index (RWI) to describe the impact of the 11 February geomagnetic storm. Energetic electron precipitation generated some additional NO_x, supplementing the original amounts that were already descending. At altitudes of 50–70 km, GOMOS observations of NO₂ showed a delayed response to the geomagnetic storm, with NO₂ being generated 3 days after the start of the storm. The delayed response and duration of NO₂ production was found to be consistent with the increase in the flux of relativistic electrons measured by GOES at geostationary orbit and by POES through relativistic electron contamination of the >16 MeV proton channel. Using the Sodankylä Ion and Neutral Chemistry model (SIC), we found that a good fit to the observed NO₂ mixing ratios at the peak of the geomagnetic storm effect was produced by a monoenergetic 1.25 MeV electron beam with a flux of $\sim 0.3 \times 10^6$ el cm⁻² sr⁻¹ s⁻¹ keV⁻¹ or with a “hard” electron spectra taken from Gaines et al. (1995) but with fluxes enhanced by a factor of 15, i.e., 8×10^4 el cm⁻² sr⁻¹ s⁻¹ for 2–6 MeV. Prior to the storm the descending NO₂ had average mixing ratio values of ~ 150 ppbv. The geomagnetic storm-induced relativistic electron precipitation event doubled the amount of NO_x descending into the stratosphere to ~ 300 ppbv after the storm.

Citation: Clilverd, M. A., A. Seppälä, C. J. Rodger, M. G. Mlynczak, and J. U. Kozyra (2009), Additional stratospheric NO_x production by relativistic electron precipitation during the 2004 spring NO_x descent event, *J. Geophys. Res.*, *114*, A04305, doi:10.1029/2008JA013472.

1. Introduction

[2] During the Arctic winter 2003–2004 several satellite and ground-based experiments observed enhanced concentrations of NO_x descending from mesospheric altitudes. As a consequence of the enhanced levels of NO_x reaching the stratosphere there was a related decrease in the levels of springtime ozone at 40 km altitudes [Randall et al., 2005]. Wintertime polar odd nitrogen, NO_x (NO + NO₂), can be produced in the thermosphere and the mesosphere by energetic particle precipitation [Brasseur and Solomon, 2005]. During periods of efficient vertical transport the NO_x can descend to the stratosphere [Siskind, 2000]. In

the upper mesosphere the NO_x is mainly in the form of NO. As the NO descends below 70 km it is converted to NO₂ [Solomon et al., 1982; Brasseur and Solomon, 2005]. The particular descent of interest here began in January 2004 [Clilverd et al., 2006], and was still observable in May 2004. Randall et al. [2005] analyzed NO₂ concentration data from three long-running solar occultation experiments, SAGE II, POAM III, and HALOE during this period. They reported unprecedented levels of springtime stratospheric NO_x (~ 45 km) as a result of the descent. Rinsland et al. [2005] also observed very high NO_x mixing ratios at 40–50 km in February/March 2004 with the ACE experiment, detecting levels as high as 1365 ppbv. The source of the NO_x that was ultimately observed at 45 km in May 2004 is still open to debate [Clilverd et al., 2007]. In this work we aim to identify additional contributions to the stratospheric NO_x produced by a geomagnetic storm in February 2004.

[3] Clilverd et al. [2006, 2007] used radio wave data that was sensitive to the ionization of NO_x at 70–90 km altitudes to show that the initial source for the NO_x observed in January 2004 was likely to be in the auroral zones in the thermosphere, and not a result of in situ production in the mesosphere. The data showed that the descent of the NO_x

¹Physical Sciences Division, British Antarctic Survey, NERC, Cambridge, UK.

²British Antarctic Survey, NERC, Cambridge, England, UK.

³Finnish Meteorological Institute, Helsinki, Finland.

⁴Department of Physics, University of Otago, Dunedin, New Zealand.

⁵NASA Langley Research Center, Hampton, Virginia, USA.

⁶Department of Atmospheric, Oceanic and Space Sciences, College of Engineering, University of Michigan, Ann Arbor, Michigan, USA.

began on 11/12 January 2004, a few days after the end of the stratospheric warming event at the end of December 2003. Seppälä *et al.* [2007a] used Global Ozone Monitoring by Occultation of Stars (GOMOS) NO₂ observations during the polar night to investigate the cause of the descending NO_x observed throughout the winter, November 2003–March 2004. They concluded that the Halloween solar proton events that occurred in late October 2003 produced significant levels of NO₂ during November and December 2003, but that a source at thermospheric altitudes was the most likely cause of the NO₂ observed descending in January 2004. However, Seppälä *et al.* [2007a] also suggested that a further enhancement of NO_x occurred in mid-February 2004 adding to the NO_x that was already descending. In this paper we analyze in detail the period in mid-February 2004 with a view to determining the contribution to the NO_x that was produced by processes driven by the 11 February geomagnetic storm, in addition to that already descending from higher altitudes.

[4] Using the Sodankylä Ion and Neutral Chemistry model (SIC), Turunen *et al.* [2009] generated NO₂ concentration profiles from four separate particle precipitation mechanisms: solar proton events, auroral electron precipitation, long-lasting relativistic electron precipitation (REP), and REP microbursts. In comparing the SIC results with GOMOS observations from the northern hemisphere polar winter 2003–2004 Turunen *et al.* [2009] concluded that the mid-February enhancement of NO₂ had the altitude profile characteristics of REP generation possibly involving an energy spectrum that contained >1 MeV electron fluxes. However, Turunen *et al.* [2009] did not identify any link to geomagnetic activity, nor what likely electron precipitation fluxes were required to reproduce the GOMOS observations.

[5] In this study we analyze the February 2004 period in detail, concentrating on the GOMOS NO₂ observations in the northern polar latitudes. We combine additional data sets to further describe the impact of the mid-February geomagnetic activity, including the SABER-observed NO 5.3 μm radiated power, and the AARDDVARK-derived radio wave index. We determine the characteristics of the geomagnetic activity that lead to the generation of enhanced NO₂ in the altitude range 40–70 km, and use the SIC model to approximately determine the energy spectrum and flux required to generate the enhanced NO₂ observed. Finally, we determine the relative impact of the geomagnetic storm-induced REP on NO₂ concentration levels in comparison with the descending NO₂ that was first observed on 11/12 January 2004.

2. Event Conditions

[6] This study concentrates on the atmospheric effects of energetic particle precipitation during a geomagnetic storm. The event conditions are shown in Figure 1, which shows solar wind conditions, and geomagnetic activity during February 2004. The solar wind shows a sharp increase in density (>20 protons cm⁻³) on 11 February 2004, followed shortly afterward by a period of high (>600 km s⁻¹) solar wind speed. Although the density increase subsides quickly, the high solar wind speed continues until 16 February, gradually returning to nondisturbed levels (~400 km s⁻¹) by 21 February. Dashed vertical lines on 11 and 16 February

2004 in Figure 1 indicate the beginning and recovery phase of the storm. These dates are also indicated in Figures 2–4 for easy comparison.

[7] Prior to the storm there was a period of relatively low solar wind speed lasting >1 day, which is consistent with a prestorm “calm” [Clilverd *et al.*, 1993; Borovsky and Steinberg, 2006] and thus suggests that this event may be driven by a coronal interaction region (CIR) rather than an incident coronal mass ejection (ICME). Additional evidence for a CIR-driven event come from the observation that February 2004 is during the declining phase of the 11-year solar cycle, and the event has a 27-day repeating occurrence pattern. Further, in geomagnetic terms the storm that occurred on 11–15 February produced only moderate *Kp* levels (*Kp*~4–6), while *D_{st}* achieved less than –100 nT only for a short period, and no increase in proton fluxes occurred during the geomagnetic storm (not shown). All of these phenomena are suggestive of a CIR-driven event rather than CME [Tsurutani *et al.*, 2006; Borovsky and Denton, 2006]. However, we note here that the atmospheric effects observed by GOMOS as a result of this CIR-driven event should be considered as an extreme event as no similar NO₂ enhancements have been found in the GOMOS 2002–2007 summary data, other than from solar proton events [Seppälä *et al.*, 2007b].

3. Experimental Setup

[8] In this paper we use NO₂ measurements from the GOMOS stellar occultation instrument [Bertaux *et al.*, 2000, 2004; Kyrölä *et al.*, 2004], on board the Envisat satellite, to investigate the signatures of NO_x descent in January/February 2004. GOMOS has the advantage over previous satellite observations of the descent of NO_x into the stratosphere in being able to measure NO₂ at altitudes up to 70 km, and in the dark polar night conditions well inside the polar vortex [Hauchecorne *et al.*, 2005, Kyrölä *et al.*, 2006]. For this study we use GOMOS dark limb (nighttime) measurements from the Northern Hemisphere (GOPR version 6.0c or later) from occultations where the star temperature was ≥6800 K. Nighttime measurements of NO₂ are a good tracer for NO_x in the stratosphere and the lower mesosphere, but not at higher altitudes where NO_x is mainly in the form of NO and the abundance of NO₂ is very low [Brasseur and Solomon, 2005]. The GOMOS data used in this study were averaged over geographic latitudes 59–80°N. We use this latitude range in order to take advantage of the same GOMOS high-temperature stars throughout as much of the February 2004 period as possible. This provides data from the polar region which contains the polar vortex (>60°N for a well developed vortex), and which also correspond to a geomagnetic latitude range from *L* > 2.8, i.e., the outer radiation belt. In some cases we restrict the latitude band to 65–75°N, with a median latitude of 70–71°N, in order to compare the GOMOS results with ion and neutral chemistry model runs at 70°N, and to maintain a consistent number of stars in the analysis throughout the study period. These geographic latitudes correspond to an *L* shell range of *L* > 3.8.

[9] To investigate the variation of high-altitude NO during February we use data from the SABER instrument. SABER is a 10 channel limb-scanning radiometer flying on

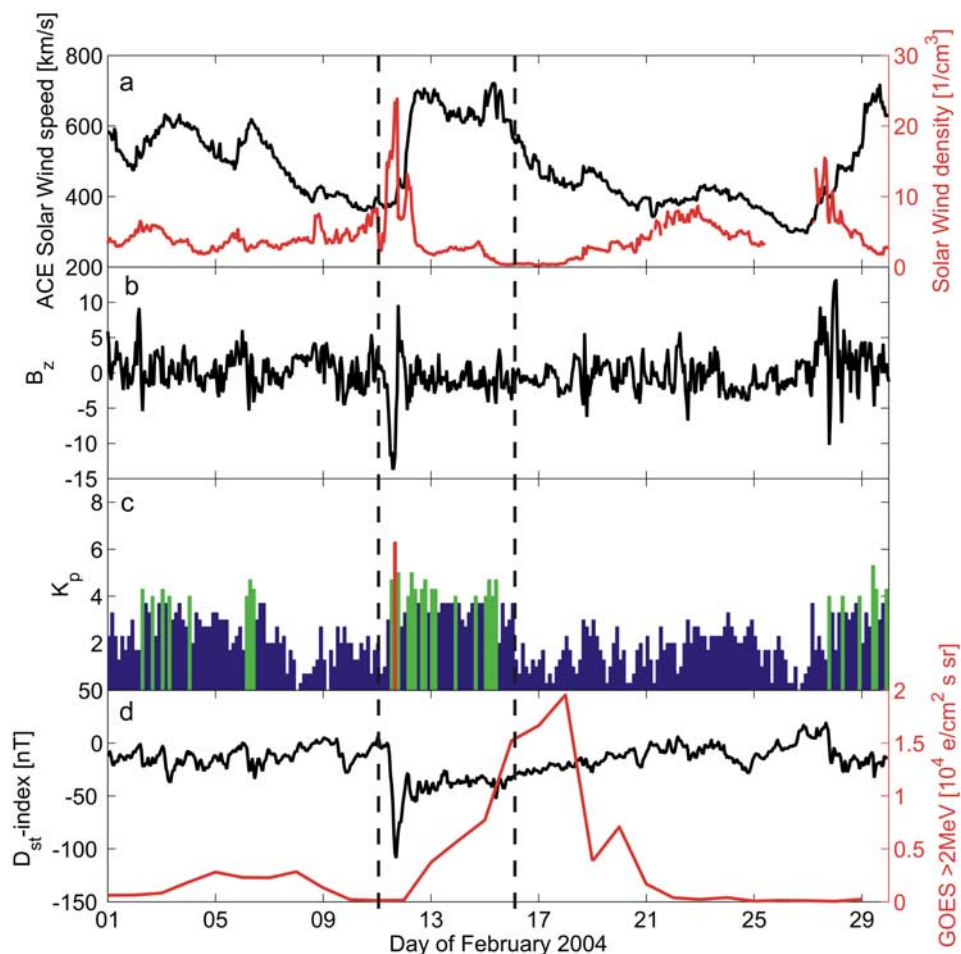


Figure 1. (a) The variation in solar wind speed and density during February 2004. (b) The variation of the B_z component of the solar wind during February 2004. (c) Three-hourly K_p index values, with disturbed times ($K_p > 5$) shown in red, moderately disturbed ($4 < K_p < 5$) in green, and quiet times ($K_p < 4$) in blue. (d) The variation in D_{st} (black line) and GOES electron flux units (>2 MeV electrons $\text{cm}^{-2} \text{s}^{-1} \text{sr}^{-1}$) in red. A significant geomagnetic disturbance can be seen starting 11 February 2004 and lasting until 16 February. There is no equivalent proton enhancement (not shown).

the NASA TIMED satellite, described by *Russell et al.* [1999]. The primary objective of SABER is to quantify the thermal structure and energy balance of the mesosphere and lower thermosphere. Every 53 s SABER scans the Earth's limb from 400 km tangent height to a height equivalent to 20 km below the hard Earth surface, simultaneously recording profiles of radiance ($\text{W cm}^{-2} \text{sr}^{-1}$) in each spectral channel. The instrument continuously scans the Earth limb, recording approximately 1600 profiles of limb radiance per channel per day. The spectral coverage of the instrument is from 1.27 to 15.4 μm [*Mlynczak et al.*, 2005]. Of particular interest for this study is the nighttime auroral 5.3 μm limb emission, and it changes promptly because of increases in NO, temperature, and also atomic oxygen. The data shown in this study is an average of the power radiated by NO in the latitude band 52–90°N – which is the SABER “high-latitude” data product of interest to us here. This geographic latitude range covers the geomagnetic L shell range from $L > 2.1$.

[10] One of the few experimental techniques which can probe the ionization at altitudes between the GOMOS and

SABER observations uses very low frequency (VLF) electromagnetic radiation, trapped between the lower ionosphere and the Earth [*Barr et al.*, 2000]. The nature of the received radio waves is largely determined by propagation between these boundaries [e.g., *Cummer*, 2000], termed “subionospheric propagation.” Here we use the AARDDVARK-derived radio wave index (RWI) which describes the variation in propagation conditions for a narrow band subionospheric transmitter (call sign NRK, 64°N, 22°W, $L = 5.6$, 37.5 kHz) located in Iceland and received at a receiver located at Ny Ålesund, Svalbard (79°N, 11°E, $L = 18.3$). Because of the geographic latitude and geomagnetic latitude of this path the propagation conditions are influenced by both the polar vortex and the outer radiation belt, and the path passes through the footprints of geostationary orbits as discussed later in section 4. Any change in the levels of either NO concentration, or ionization rates due to particle precipitation, in the 70–90 km altitude range can be identified in the RWI [*Clilverd et al.*, 2007]. The Ny Ålesund site is part of the Antarctic-Arctic Radiation-belt Dynamic Deposition VLF

Atmospheric Research Konsortia (AARDDVARK); see *Clilverd et al.* [2009] for more details.

[11] Radiation belt particle data is provided by instruments onboard the Geostationary Operational Environmental Satellite (GOES) and Polar Operational Environmental Satellite (POES) Program spacecraft, which are a cooperative effort between NASA and the National Oceanic and Atmospheric Administration (NOAA). The Space Environment Monitor instrument onboard GOES 11 provides 1-min >2 MeV electron fluxes at a nominal fixed L shell of $L = 6.6$. The GOES >2 MeV channel primarily responds to trapped outer zone particles. In practice the geostationary orbit is not at a constant L , and so we use to daily average to compensate for the factor of ~ 5 variation during a normal “quiet time” orbit. The Polar Orbiting Environmental Satellites (POES) (formerly known as TIROS for Television and InfraRed Observation Satellite) carry the Space Environment Monitor-2 instrument, which observes trapped and precipitating (loss cone) electrons and protons. In this study we make use of measurements from the POES spacecraft NOAA 15, 16 and 17. As POES are located in polar orbits, they sweep through a range of L shells, sampling both the inner and outer radiation belts. POES instruments measure trapped and loss cone electron integral fluxes for energy thresholds of >30 , >100 and >300 keV. Here we make use of two POES data products, the POES radiation belt indices (available from http://www.swpc.noaa.gov/ftpdir/lists/bi/old_bi/) and the POES Space Environment Monitor-2 16-s average measurements (available from <http://poes.ngdc.noaa.gov/data/avg/>). The radiation belt indices are a daily value indicating the ratio of the daily trapped particle counts to their corresponding 1-year summed average for each energy channel. The indices are subdivided by L to provide inner ($L < 2.0$), slot ($2.0 \leq L < 2.5$), and outer ($L \geq 2.5$) radiation belt indices.

[12] The POES Space Environment Monitor-2 suite includes a >300 keV loss cone telescope and an omnidirectional proton integral energy channel with energy threshold >16 MeV which responds to trapped >0.8 MeV electrons as a “contaminant” in the absence of any significant proton fluxes [*Sandanger et al.*, 2007]. We use the 16-s average measurements from the proton integral energy channel to detect trapped relativistic electrons, as there was no solar proton event in this period. The relative detection efficiency of the POES >16 MeV proton channel is 50% for 1.5 MeV electrons and climbs to 100% for 2 MeV electrons [*Sandanger et al.*, 2007], and as such this data is a very useful representation of trapped relativistic electron populations (outside of solar proton events). As the fluxes are being measured at low altitudes they represent a measurement of particles closer to the loss cone (smaller pitch angles) than the fluxes measured by GOES. So, an increase in the POES omnidirectional detector does indicate when particles have been scattered from near-equatorial pitch angles to closer to the loss cone, which is consistent with the hypothesis that precipitation is likely to be occurring.

4. Results

[13] In Figure 2 we show a composite picture which combines data from all three experimental techniques during

the period January–February 2004. Figure 2 (top) shows the daily average NO radiated power from SABER in the northern polar region (52 – 90° N) in the altitude range 100–200 km, starting from 16 January 2004. The values obtained during January and February varied from 1 to 7.6×10^{10} W with high levels observed over 16–27 January, and 11–16 February. The start of the first period of enhanced NO radiated power was not captured in the SABER observations. However, the second period is clearly associated with the geomagnetic storm that began on 11 February, and lasted as long as the period of high solar wind speeds, finishing on 15 February. As this change is in step with the 15 μ m power for SABER CO₂ data (not shown) we conclude that the NO radiated power increase is likely to be due to storm-induced changes in temperature, rather than an increase in NO due to ionization from low-energy electron precipitation. Figure 2 (middle) shows the daily AARDDVARK RWI, values varied from -15 to 5 dB during January and February, with an extended period of high levels (denoting enhanced ionospheric ionization levels in the altitude range 70–90 km) from 11 January to 5 February, and then a second period from 11 to 19 February. The first period of enhanced RWI has been associated with the ionization of descending NO_x by Lyman- α as a result of strong vertical descent associated with a strengthening of the underlying polar vortex [*Clilverd et al.*, 2006, 2007]. The second period of enhanced RWI is coincident with the 11–16 February geomagnetic storm, although lasting longer than the period of high solar wind speed, and peaking in magnitude at the time that the SABER event finishes.

[14] Figure 2 (bottom) shows the daily averaged GOMOS nighttime NO₂ mixing ratios from 30 to 70 km and 59–80°N. The average mixing ratios range from 0 to 600 ppbv during January and February 2004, with a gradually descending enhancement of NO_x starting at around 70 km on 11 January reaching ~ 45 km by the end of February. The origin of this descending feature has been ascribed to auroral-altitude (>90 km) NO_x [*Clilverd et al.*, 2007] descending because of strong vertical transport of subsiding polar air [*Randall et al.*, 2005]. The enhancement of NO₂ weakens after 5 February, but is strongly enhanced over a large range of altitudes from 14 to 19 February coincident with, and following, the geomagnetic storm shown in Figure 1. *Seppälä et al.* [2007a] and *Turunen et al.* [2009] identified this increase in NO₂ in the GOMOS data as being due to in situ generation of NO_x by energetic electron precipitation, suggesting relativistic electron precipitation as the most likely source because of the altitude at which the NO₂ was generated. In this paper we study this period in detail and attempt to quantify the contribution of the energetic electron precipitation to the NO_x levels that were eventually observed at 40 km by *Randall et al.* [2005] and *Rinsland et al.* [2005].

[15] One interesting difference in the geomagnetic storm as seen in the SABER NO radiated power, the AARDDVARK RWI, and the GOMOS NO₂ data is in the timing of the event at the different altitudes that the data sets represent. At altitudes >100 km the storm effect is observed by SABER from 11 to 16 February. However, at 50–70 km the storm effect is seen by GOMOS from 14 to 19 February. Starting later and finishing later than the SABER event. The 70–90 km RWI also confirms the later finish date at altitudes

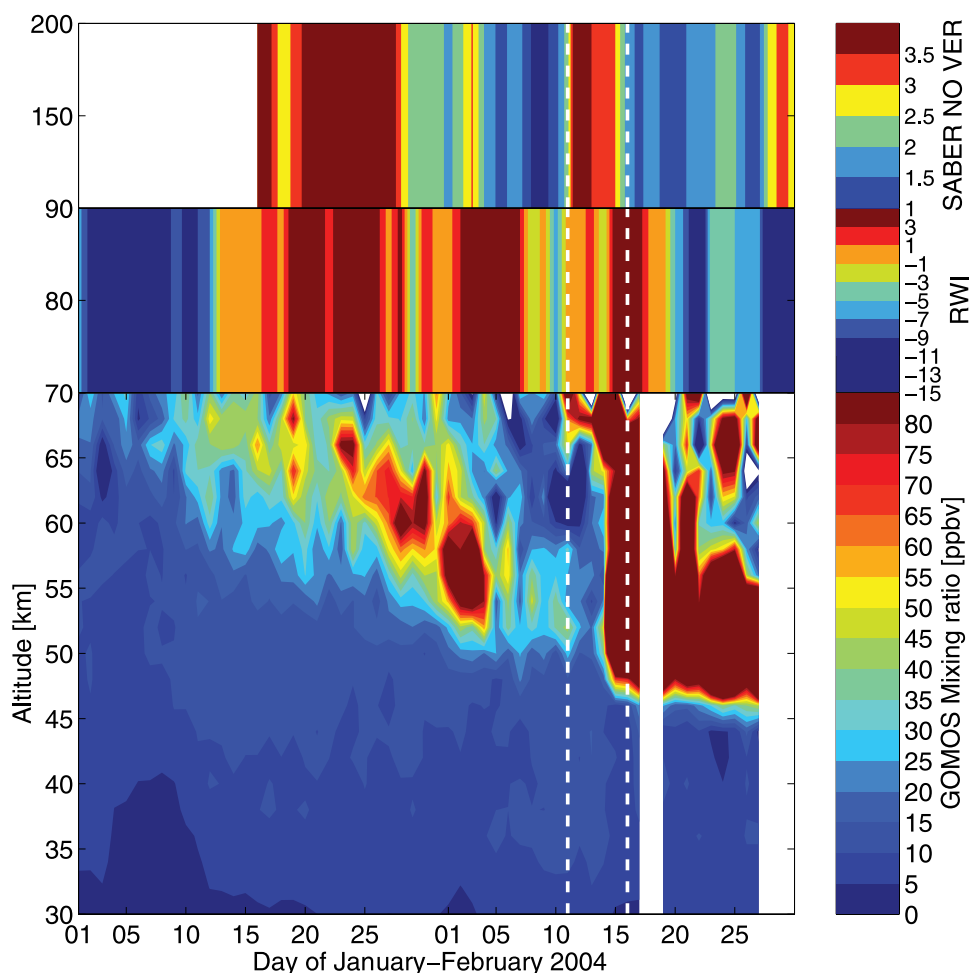


Figure 2. A composite showing (top) the SABER NO 5.3 μm radiated power (100–200 km), (middle) AARDDVARK radio wave index (RWI, 70–90 km), and (bottom) average 59–80° latitude GOMOS NO₂ mixing ratio (30–70 km) during January and February 2004. Enhanced NO₂, RWI, and NO can be seen from 11 January 2004, followed by another enhancement from 11 February 2004. Recovery to the second enhancement takes ~ 5 days at >100 km (denoted by the dashed vertical lines) but continues to the end of the plot window at ~ 50 km.

<100 km. Of particular interest to this paper is why the NO₂ generated at 50–70 km altitudes is so delayed with respect to the storm start.

[16] Figure 3 gives an insight into why the two altitudes respond at such different times. Figure 3 (top) shows the variation of the POES outer radiation belt ($L > 2.5$) daily index for >30 keV electrons, and a daily average of the GOES >2 MeV trapped electron fluxes ($L = 6.6$). Precipitating 30 keV electrons produce ionization at >90 km altitudes [Rees, 1989; Turunen *et al.*, 2009], while precipitating 2 MeV electrons produce ionization at >50 km. Thus the POES >30 keV electron index is more useful for comparison with SABER data, while the GOES >2 MeV electron fluxes are more useful for comparison with the GOMOS data. Figure 3 (bottom) shows the variation of the POES count rates in February 2004 for the ~ 1.5 MeV omnidirectional detector and the >300 keV loss cone detector, measured at $L = 4.5$, i.e., in the heart of the outer radiation belt. In both Figure 3 (top) and Figure 3 (bottom) we can see that the POES outer radiation belt index and the

>300 keV loss cone counts respond at the beginning of the storm period (11 February), while the GOES >2 MeV trapped fluxes and the POES ~ 1.5 MeV omnidirectional detector respond later, and peak after, the POES outer radiation belt index and the >300 keV loss cone counts. We note here that the increase in GOES fluxes indicates an increase in trapped fluxes which may lead to higher precipitating fluxes. The low-altitude POES omnidirectional detector measurements, which also show an increase, are consistent with this hypothesis.

[17] In Figure 4 we show POES data plotted as a function of L shell versus date in February 2004. The 16-s average measurements from all 3 POES spacecraft are processed to create mean flux measurements in bins which are 3 h and $0.25 L$ wide, with measurements taken from inside the South Atlantic Magnetic Anomaly removed. Figure 4 (top) shows values from the POES >16 MeV omnidirectional proton channel which responds to relativistic electrons. We follow the approach of previous authors in describing this as a ~ 1.5 MeV electron channel [Sandanger

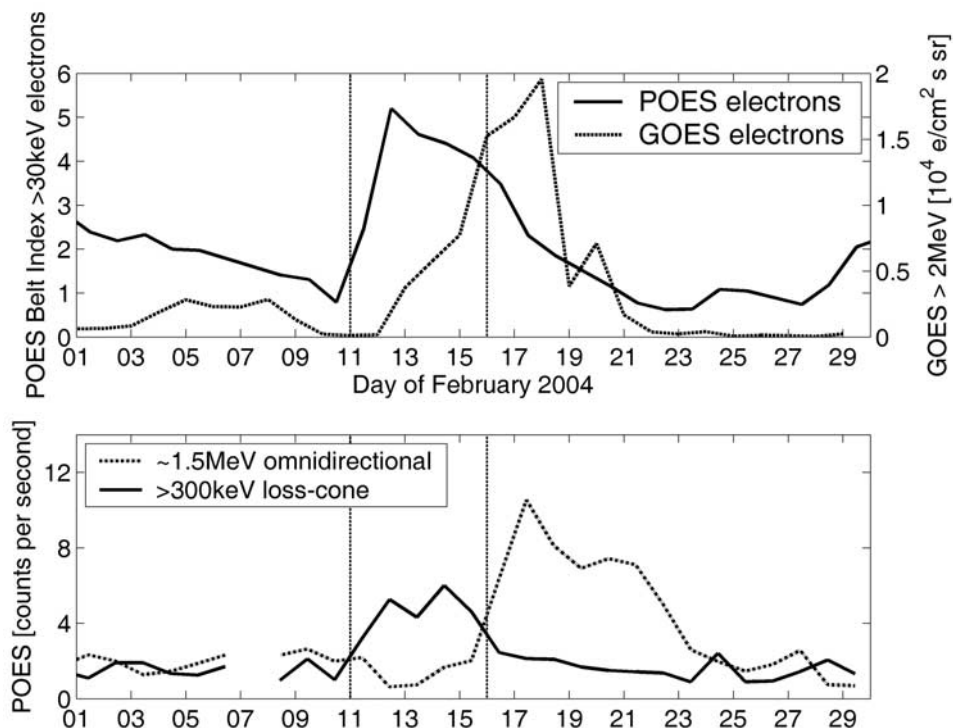


Figure 3. (top) The variation of the POES outer radiation belt index (>30 keV electrons) and the daily averaged GOES 12 >2 MeV electron flux in February 2004. The outer radiation belt index shows an immediate response to the geomagnetic storm on 11 February, peaking on 12 February, while the >2 MeV fluxes gradually start to increase 2 days after onset of the geomagnetic storm, peaking on 18 February. (bottom) The variation of the POES >1.5 MeV omnidirectional detector and the >300 keV loss cone detector for $L = 4.5$ during February 2004.

et al., 2007], although as noted above the detection efficiency of this proton channel for relativistic electrons is energy dependent. The geomagnetic storm of 11 February produces very low fluxes of relativistic electron contamination initially, but high relativistic electron fluxes at $L > 4$ from 14 to 21 February, consistent with the period of GOMOS NO₂ production. Figure 4 (middle) shows the POES >300 keV loss cone electron flux, while Figure 4 (bottom) shows that the POES >30 keV loss cone electron flux. The loss cone fluxes undergo a sudden enhancement at $L > 4$ on 11 February, lasting until 16 February, contiguous with high solar wind speeds during the geomagnetic storm, and SABER NO radiated power observations. Thus from Figures 3 and 4 we conclude that enhanced fluxes of trapped relativistic electrons are generated at $L > 4$ and as far out as $L \sim 7$, as the effect is seen clearly in the GOES data at $L = 6.6$. The generation is delayed by ~ 3 – 4 days in respect of the start of the storm, which is consistent with acceleration of seed populations of low-energy electrons by wave-particle interactions or radial diffusion, and consistent with CIR-driven storms [Tsurutani *et al.*, 2006]. Although the loss cone measurements at >30 keV and >300 keV do not show any significant enhancements from 16 to 19 February, the enhancement of the quasi-trapped >1.5 MeV fluxes is consistent with the results from previous studies of this period in suggesting that the increase in GOMOS NO₂ is a result of increased relativ-

istic electron precipitation into the atmosphere [Seppälä *et al.*, 2007a; Turunen *et al.*, 2009].

5. Modeling the REP-Generated NO_x

[18] The detailed impact of the geomagnetic storm of 11–16 February 2004 on the NO₂ altitude profiles in the latitude range 65°–75°N, which is where the maximum NO₂ enhancement was observed, is shown in Figure 5. Figure 5 (top) identifies three critical periods: before, during, and after the storm. Before the storm, from 1 to 5 February, the average NO₂ profile is represented by a maximum in mixing ratio at ~ 55 km, with values of ~ 150 ppbv. There is little NO₂ below 50 km or above 60 km. During the latter part of the storm, from 15 to 20 February, the average NO₂ profile is represented by a maximum in mixing ratio between 52 and 56 km, with values of >500 ppbv. There is some NO₂ as low as ~ 47 km, but significant amounts occur over a larger altitude range than before the storm, up to 65 km in altitude. After the storm, from 25 to 29 February, the NO₂ profile is represented by a maximum in mixing ratio at ~ 52 km, with values of ~ 300 ppbv, but the altitude range over which significant NO₂ occurs has again reduced to ~ 10 km.

[19] Figure 5 (bottom) shows 2-day averages of the NO₂ mixing ratio (circles) measured at the peak of the descending feature, where the altitude of the measurement is shown by the squares in the same plot. Following a period at the

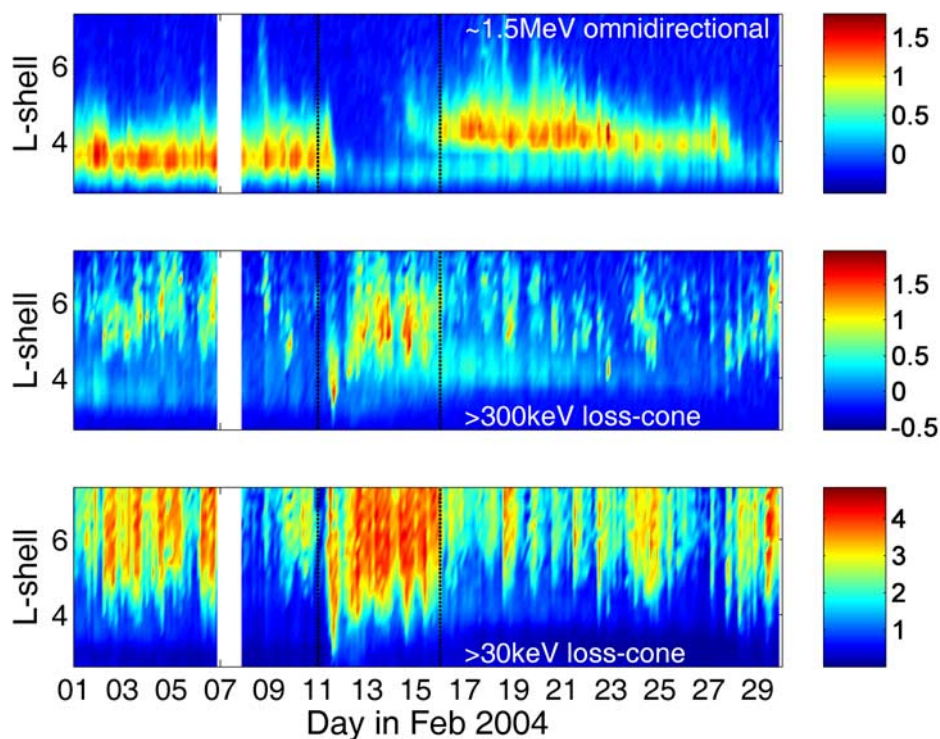


Figure 4. (top) The POES >16 MeV proton channel during February 2004, which we use here to identify relativistic electrons (>0.8 MeV). The geomagnetic storm produces high relativistic electron fluxes at $L > 4$ from 14 to 21 February, consistent with the period of GOMOS NO₂ production. (middle) The POES >300 keV loss cone electron flux variation with L shell. (bottom) The POES >30 keV loss cone electron flux variation with L shell. The fluxes show a sudden enhancement on 11 February, lasting until 16 February, contiguous with high solar wind speeds during the geomagnetic storm, and SABER NO 5.3 μm radiated power observations. All values are in counts/s.

beginning of January, where the mixing ratio values are steadily increasing because of conversion from NO to NO₂ with decreasing altitude [Brasseur and Solomon, 2005], the mixing ratios then remain at a quasi-constant value of ~ 150 ppbv until 7 February. Between 8 and 13 February there is a gap in the occurrence of measurements in the 65° – 75°N latitude range. However, GOMOS observations in Figure 2 show that no immediate effect of the geomagnetic storm on NO₂ is observed at the onset of the storm. During and just after the geomagnetic storm (14–18 February) the mixing ratios increase to 600 ppbv before settling back down to ~ 300 ppbv late in February. The loss of ~ 200 ppbv of NO₂ at the end of the geomagnetic storm is consistent with the removal of NO₂ into reservoir species such as ClONO₂ [von Clarmann et al., 2005; López-Puertas et al., 2005]. Delayed ClONO₂ increases were observed by MIPAS instruments following the October 2003 solar proton events as a result of temporal development of active chlorine during the storm, with subsequent buffering into its inactive reservoir (ClONO₂) [von Clarmann et al., 2005]. Reactions such as this may account for the observed loss of NO₂ at the end of the geomagnetic storm; loss by photolysis alone seems unable to explain the rapid temporal variability shown.

[20] After 20 February the NO₂ mixing ratios remain at an elevated and quasi-constant level of ~ 300 ppbv. From these measurements we conclude that in overall terms the

geomagnetic storm doubled the amount of NO_x that was descending toward the stratosphere. The low-altitude, high-latitude, and wintertime conditions for this event mean that any loss of NO_x by photolysis is minimal, and the NO_x should be able to survive long enough to descend to low altitudes with the poststorm mixing ratios, which is consistent with the observations of Randall et al. [2005] for April/May 2004 at ~ 40 km altitudes.

[21] In this section we use the Sodankylä Ion and Neutral Chemistry model (SIC) to investigate what energy spectrum and flux of precipitating electrons are required to generate the altitude profile of NO₂ observed by GOMOS at the peak of the geomagnetic storm effect. The SIC model is a 1-D chemical model designed for ionospheric D region studies, solving the concentrations of 65 ions, including 29 negative ions, and 15 neutral species at altitudes across 20–150 km. This study makes use of SIC version 6.9.0. A detailed overview of the model was given in Verronen et al. [2005], building on original work by Turunen et al. [1996] and Verronen et al. [2002]. In the SIC model several hundred reactions are implemented, plus additional external forcing due to solar radiation (1–422.5 nm), electron and proton precipitation, and galactic cosmic radiation. Initial descriptions of the model are provided by Turunen et al. [1996], with neutral species modifications described by Verronen et al. [2002]. Solar flux is calculated with the SOLAR2000

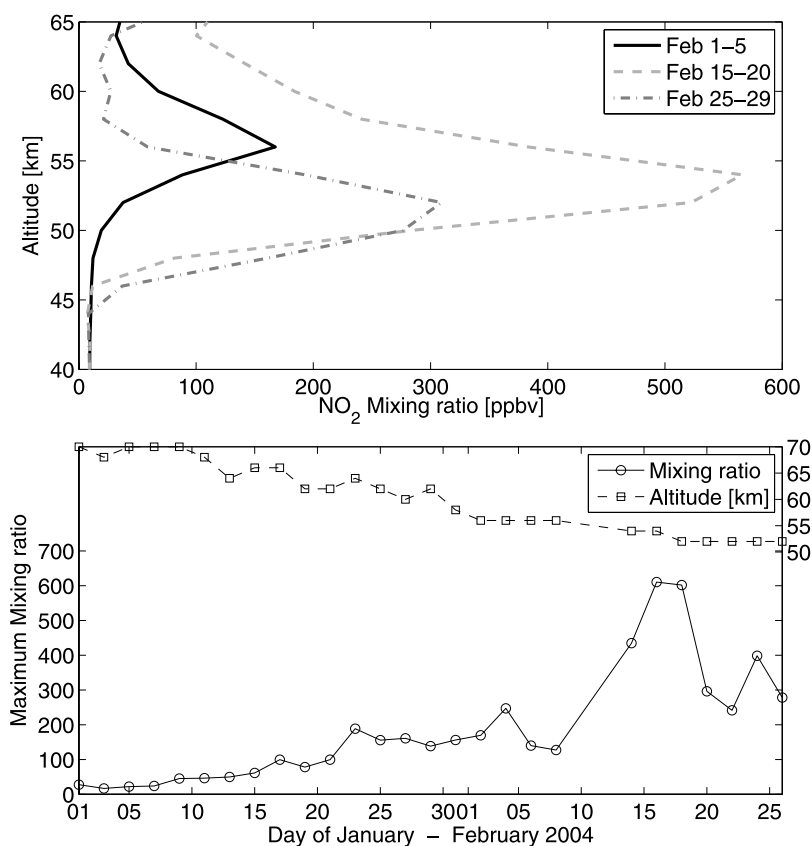


Figure 5. (top) Showing the variation in the latitude range 65–75°N of the NO₂ mixing ratio with altitude during three selected periods during February 2004. The blue line represents observations made before the onset of the geomagnetic storm period, the green line is during the geomagnetic storm, and the red line is after the end of the storm. (bottom) The 2-day average mixing ratio (circles) at the peak of the descending NO_x feature (squares represent the altitude of the peak), measured during January and February. There was a gradual increase in mixing ratio from low levels at the start of January, leveling off at ~150 ppbv between 22 January and 5 February, then increasing from 14 February, leveling off again at ~300 ppbv by the end of the month, consistent with Figure 5 (top).

model (version 2.27) [Tobiska *et al.*, 2000]. The scattered component of solar Lyman- α flux is included using the empirical approximation given by Thomas and Bowman [1986]. The SIC code includes vertical transport [Chabrilat *et al.*, 2002] which takes into account molecular [Banks and Kockarts, 1973] and eddy diffusion with a fixed eddy diffusion coefficient profile. The background neutral atmosphere is calculated using the MSISE-90 model [Hedin, 1991] and tables given by Shimazaki [1984]. Transport and chemistry are advanced in intervals of 5 or 15 min. While within each interval exponentially increasing time steps are used because of the wide range of chemical time constants of the modeled species.

[22] In reality the method used here was one of iteration, with a general target of keeping assumptions to a minimum. Initially a simple energy spectrum for the electron precipitation is assumed, along with a precipitation flux. Then the altitude-dependent ionization rate is calculated making use of the expressions given by Rees [1989, chap. 3], with effective electron ranges taken from Goldberg and Jackman [1984]. Finally we ran the SIC model with the ionization rates imposed to determine the amount of NO_x that would be generated by that amount of ionization. As a result of this

iterative process, we identified that the ionization rate profile from a monoenergetic beam of 1.25 MeV electrons with a flux of $0.3 \times 10^6 \text{ el cm}^{-2} \text{ sr}^{-1} \text{ s}^{-1} \text{ keV}^{-1}$ was able to reproduce the GOMOS observations. Figure 6 shows the ionization rate profile from the final electron beam parameters. The energy of the electrons strongly defines the altitude of the peak ionization rate, although it should be noted that substantial ionization occurs at altitudes above the peak even with a monoenergetic beam, because of scattering on the way through the atmosphere. For comparison we also show the ionization rate profile generated by the spectrum shown in Figure 3 (18 May 1992, 2247 UT) of Gaines *et al.* [1995] and discussed by Turunen *et al.* [2009], but with the fluxes multiplied by a factor of 15. The resultant ionization rate profile is very similar to the monoenergetic beam apart from an increased contribution at ~15 km due to the ~5 MeV electrons in the Gaines *et al.* [1995] spectra.

[23] The concentration of NO₂ in the altitude range 40–70 km is shown in Figure 7. NO₂ was generated by imposing the ionization rates from either the monoenergetic beam of 1.25 MeV electrons, or the enhanced Gaines *et al.* [1995] spectra, on the SIC calculations made at 70°N, 0°E

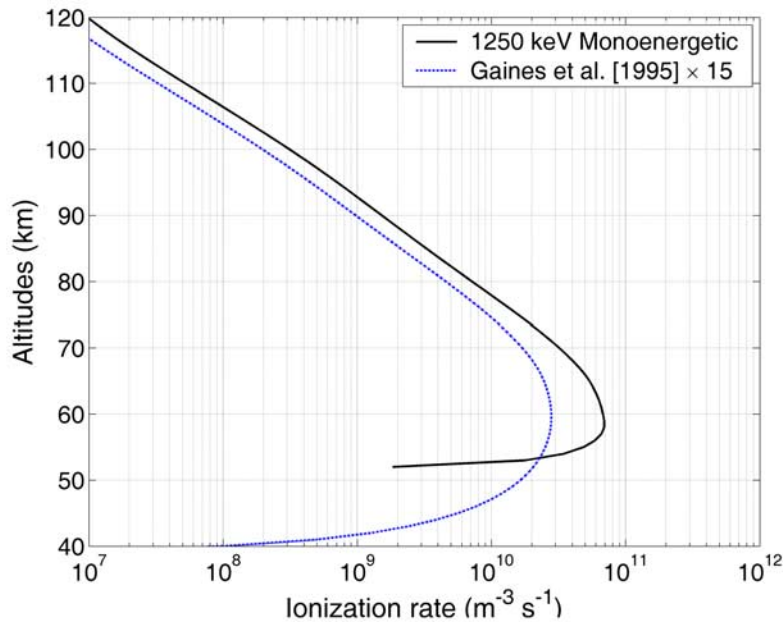


Figure 6. The ionization rate generated by a monoenergetic beam of 1.25 MeV electrons, and a $15 \times$ *Gaines et al.* [1995] storm time spectra, imposed on the SIC model to reproduce the observed NO₂ mixing ratios that occurred during the geomagnetic storm of 15–20 February 2004.

for 3 days. The SIC NO₂ variation with altitude 4 days after the ionization period is indicated by the black solid line. In comparison, the largest nighttime GOMOS NO₂ average values from 65°–75°N are shown by the dashed

line. The gray line represents the SIC model NO₂ profile without electron precipitation forcing. The GOMOS data during the geomagnetic storm is reasonably modeled by the effects of either the monoenergetic 1.25 MeV electron

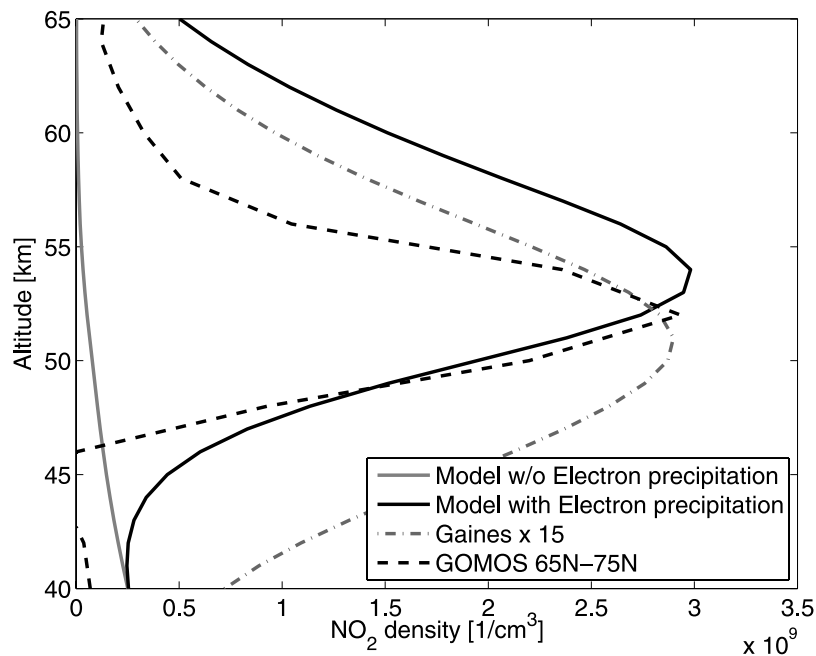


Figure 7. The altitude variation of the NO₂ densities observed by GOMOS during the maximum effect of the geomagnetic storm (dashed line) compared with the calculated SIC quiet time NO₂ concentrations (gray line) and the results from the monoenergetic 1.25 MeV REP forcing with a flux of $0.3 \times 10^6 \text{ el cm}^{-2} \text{ sr}^{-1} \text{ s}^{-1} \text{ keV}^{-1}$ (black line), and the enhanced *Gaines et al.* [1995] spectra (dot-dashed line). Good agreement is obtained between the GOMOS data and the SIC results using these levels of REP.

precipitation, or the 40 times enhanced Gaines spectra, at altitudes 45–60 km. The 1.25 MeV monoenergetic flux of 0.3×10^6 el cm⁻² sr⁻¹ s⁻¹ keV⁻¹ produces the peak values of 500 ppbv when taking into account the 150 ppbv that was already present prior to the geomagnetic storm.

[24] The estimated fluxes for this event can be put into context by comparing them with satellite measurements of electron precipitation fluxes made during geomagnetic storms. The *Gaines et al.* [1995] bounce loss cone (BLC) spectra from a storm time period in 18 May 1992 at 2247 UT gave 5.3×10^3 el cm⁻² sr⁻¹ s⁻¹ for 2–6 MeV between $L = 3.5$ and 4.0. *Gaines et al.* [1995] showed that these fluxes were larger than the drift loss cone (DLC) fluxes at the same time, i.e., at electron precipitation energies which are capable of reaching ~50 km altitudes the BLC fluxes have been observed to be 200% of the DLC fluxes. Daily average BLC and DLC flux comparisons shown by *Gaines et al.* [1995] also suggest that they can be about the same at the high-energy end (>2 MeV) during storms. Using ~11 years of data, the SAMPEX observations of DLC fluxes for 2–6 MeV electrons between $L = 3$ and 4.5 are typically $\sim 10^5$ el cm⁻² sr⁻¹ s⁻¹ during long-lived, storm time, flux enhancements [*Baker et al.*, 2004]. The Gaines x 15 BLC spectra from a flux enhancement event (used in this modeling study) represents ~80% of the DLC flux (>2 MeV) seen by SAMPEX during the storm period studied here [*Baker et al.*, 2004].

6. Summary

[25] During the much discussed descent of polar NO_x in the northern hemisphere spring 2004 [*Randall et al.*, 2005; *Rinsland et al.*, 2005; *Clilverd et al.*, 2006] a geomagnetic storm occurred on 11–16 February 2004 that appeared to generate some additional NO_x, supplementing the original amounts that were already descending. At altitudes >70 km SABER observations and AARDDVARK radio wave data showed an immediate affect of the geomagnetic storm which coincide with either the generation of NO by relatively low energy electron precipitation (~30 keV) or with enhanced temperatures at altitudes >100 km, or both, probably associated with direct input from the solar wind. The enhancement of SABER NO radiated power ended when the solar wind speed fell below 600 km⁻¹ 4–5 days after the start of the storm, but the 70–90 km AARDDVARK radio wave data continued to show a response for a further 4 days, recovering on 19 February.

[26] At altitudes 50–70 km GOMOS observations of NO₂ showed a delayed response to the geomagnetic storm with NO₂ being generated from 14 to 19 February. The delayed response and duration of NO₂ production was found to be consistent with the increase in the flux of trapped relativistic electrons measured by GOES at geostationary orbit and by POES through relativistic electron contamination of the >16 MeV proton channel. The delayed enhancement of radiation belt relativistic electron fluxes is consistent with the acceleration of seed populations of low-energy electrons after the onset of the storm, reaching relativistic energies after several days [*Horne*, 2002; *Horne et al.*, 2005]. The accelerated electrons are then presumably lost to the atmosphere by particle precipitation mechanisms also driven by the geomagnetic storm [e.g., *Rodger et al.*, 2007]. Using

the SIC model we found that a good fit to the observed NO₂ mixing ratios at the peak of the geomagnetic storm effect was produced by either a monoenergetic 1.25 MeV electron beam with a flux of $\sim 0.3 \times 10^6$ el cm⁻² sr⁻¹ s⁻¹ keV⁻¹ or a 15 times enhanced *Gaines et al.* [1995] bounce loss cone spectra which gives fluxes of 8×10^4 el cm⁻² sr⁻¹ s⁻¹ for 2–6 MeV. The geomagnetic storm that generated this upper stratospheric NO_x was driven by a CIR-type storm with high solar wind speeds, moderate Kp , and a 3-day delayed buildup of >2 MeV electron fluxes at geostationary orbit. The NO_x was generated by precipitating electron fluxes that lasted for ~3 days, and our observations suggest that this geomagnetic storm was particularly geoeffective in terms of relativistic electron loss into the atmosphere.

[27] Prior to the storm the descending NO₂ had mixing ratio values of ~150 ppbv. After the storm the descending NO₂ had mixing ratios of ~300 ppbv, which leads us to conclude that the geomagnetic storm-induced REP event doubled the amount of NO_x descending into the stratosphere, in comparison with the original event that started in January 2004. However, during the peak of the relativistic electron precipitation effect the maximum mixing ratios observed were ~500 ppbv. We speculate that part of the observed ~200 ppbv loss of NO₂ at the end of the geomagnetic storm could be caused by the removal of NO₂ into reservoir species such as ClONO₂.

[28] **Acknowledgments.** M.A.C. would like to thank Glenda Harden at BAS for her valuable support in the development of this work. A.S. thanks the Academy of Finland for their support through the EPPIC project. The authors would like to thank the SABER and GOMOS science teams for useful and informative discussions regarding this work. We are grateful to NASA and the National Oceanic and Atmospheric Administration (NOAA) for the observations provided by the Polar Operational Environmental Satellite (POES) and Geostationary Operational Environmental Satellite Program (GOES) programs.

[29] Zuyin Pu thanks Michael Denton and another reviewer for their assistance in evaluating this paper.

References

- Baker, D. N., S. G. Kanekal, X. Li, S. P. Monk, J. Goldstein, and J. L. Burch (2004), An extreme distortion of the Van Allen belt arising from the ‘Hallowe’en’ solar storm in 2003, *Nature*, *432*, 878–881, doi:10.1038/nature03116.
- Banks, P. M., and G. Kockarts (1973), *Aeronomy*, vol. B, chap. 15, Part B, pp. 32–63, Academic, New York.
- Barr, R., D. L. Jones, and C. J. Rodger (2000), ELF and VLF radio waves, *J. Atmos. Sol. Terr. Phys.*, *62*(17–18), 1689–1718, doi:10.1016/S1364-6826(00)00121-8.
- Bertaux, J. L., E. Kyrölä, and T. Wehr (2000), Stellar occultation technique for atmospheric ozone monitoring: GOMOS on Envisat, *Earth Obs. Q.*, *67*, 17–20.
- Bertaux, J. L., et al. (2004), First results on GOMOS/Envisat, *Adv. Space Res.*, *33*, 1029–1035, doi:10.1016/j.asr.2003.09.037.
- Borovsky, J. E., and M. H. Denton (2006), Differences between CME-driven storms and CIR-driven storms, *J. Geophys. Res.*, *111*, A07S08, doi:10.1029/2005JA011447.
- Borovsky, J. E., and J. T. Steinberg (2006), The “calm before the storm” in CIR/magnetosphere interactions: Occurrence statistics, solar wind statistics, and magnetospheric preconditioning, *J. Geophys. Res.*, *111*, A07S10, doi:10.1029/2005JA011397.
- Brasseur, G., and S. Solomon (2005), *Aeronomy of the Middle Atmosphere*, 3rd ed., D. Reidel, Dordrecht, Netherlands.
- Chabrilat, S., G. Kockarts, D. Fonteyn, and G. Brasseur (2002), Impact of molecular diffusion on the CO₂ distribution and the temperature in the mesosphere, *Geophys. Res. Lett.*, *29*(15), 1729, doi:10.1029/2002GL015309.
- Clilverd, M. A., T. D. G. Clark, A. J. Smith, and N. R. Thomson (1993), Observation of a decrease in midlatitude whistler-mode signal occurrence prior to geomagnetic storms, *J. Atmos. Terr. Phys.*, *55*, 1479–1485, doi:10.1016/0021-9169(93)90113-D.

- Clilverd, M. A., A. Seppälä, C. J. Rodger, P. T. Verronen, and N. R. Thomson (2006), Ionospheric evidence of thermosphere-to-stratosphere descent of polar NO_x, *Geophys. Res. Lett.*, *33*, L19811, doi:10.1029/2006GL026727.
- Clilverd, M. A., A. Seppälä, C. J. Rodger, N. R. Thomson, J. Lichtenberger, and P. Steinbach (2007), Temporal variability of the descent of high-altitude NO_x, *J. Geophys. Res.*, *112*, A09307, doi:10.1029/2006JA012085.
- Clilverd, M. A., et al. (2009), Remote sensing space weather events: Antarctic-Arctic Radiation-belt (Dynamic) Deposition-VLF Atmospheric Research Konsortium network, *Space Weather*, doi:10.1029/2008SW000412, in press.
- Cummer, S. A. (2000), Modeling electromagnetic propagation in the Earth-ionosphere waveguide, *IEEE Trans. Antennas Propag.*, *48*(9), 1420–1429, doi:10.1109/8.898776.
- Gaines, E., D. Chenette, W. Imhof, C. Jackman, and J. Winningham (1995), Relativistic electron fluxes in May 1992 and their effect on the middle atmosphere, *J. Geophys. Res.*, *100*(D1), 1027–1033, doi:10.1029/94JD02615.
- Goldberg, R. A., and C. H. Jackman (1984), Nighttime auroral energy deposition in the middle atmosphere, *J. Geophys. Res.*, *89*(A7), 5581–5596, doi:10.1029/JA089iA07p05581.
- Hauchecorne, A., et al. (2005), First simultaneous global measurements of nighttime stratospheric NO₂ and NO₃ observed by Global Ozone Monitoring by Occultation of Stars (GOMOS)/Envisat in 2003, *J. Geophys. Res.*, *110*, D18301, doi:10.1029/2004JD005711.
- Hedin, A. E. (1991), Extension of the MSIS thermospheric model into the middle and lower atmosphere, *J. Geophys. Res.*, *96*, 1159–1172, doi:10.1029/90JA02125.
- Horne, R. B. (2002), The contribution of wave-particle interactions to electron loss and acceleration in the Earth's radiation belts during geomagnetic storms, in *Review of Radio Science: 1999–2002 URSI*, edited by W. R. Stone, pp. 801–828, John Wiley, New York.
- Horne, R. B., et al. (2005), Wave acceleration of electrons in the Van Allen radiation belts, *Nature*, *437*, 227–230, doi:10.1038/nature03939.
- Kyrölä, E., et al. (2004), GOMOS on Envisat: An overview, *Adv. Space Res.*, *33*, 1020–1028, doi:10.1016/S0273-1177(03)00590-8.
- Kyrölä, E., et al. (2006), Nighttime ozone profiles in the stratosphere and mesosphere by the Global Ozone Monitoring by Occultation of Stars on Envisat, *J. Geophys. Res.*, *111*, D24306, doi:10.1029/2006JD007193.
- López-Puertas, M., B. Funke, S. Gil-López, T. von Clarmann, G. P. Stiller, M. Höpfner, S. Kellmann, H. Fischer, and C. H. Jackman (2005), Observation of NO_x enhancement and ozone depletion in the Northern and Southern Hemispheres after the October–November 2003 solar proton events, *J. Geophys. Res.*, *110*, A09S43, doi:10.1029/2005JA011050.
- Mynczak, M. G., et al. (2005), Energy transport in the thermosphere during the solar storms of April 2002, *J. Geophys. Res.*, *110*, A12S25, doi:10.1029/2005JA011141.
- Randall, C. E., et al. (2005), Stratospheric effects of energetic particle precipitation in 2003–2004, *Geophys. Res. Lett.*, *32*, L05802, doi:10.1029/2004GL022003.
- Rees, M. H. (1989), *Physics and Chemistry of the Upper Atmosphere*, Cambridge Univ. Press, Cambridge, U. K.
- Rinsland, C. P., C. Boone, R. Nassar, K. Walker, P. Bernath, J. C. McConnell, and L. Chiou (2005), Atmospheric Chemistry Experiment (ACE) Arctic stratospheric measurements of NO_x during February and March 2004: Impact of intense solar flares, *Geophys. Res. Lett.*, *32*, L16S05, doi:10.1029/2005GL022425.
- Rodger, C. J., M. A. Clilverd, N. R. Thomson, R. J. Gamble, A. Seppälä, E. Turunen, N. P. Meredith, M. Parrot, J. A. Sauvaud, and J.-J. Berthelier (2007), Radiation belt electron precipitation into the atmosphere: Recovery from a geomagnetic storm, *J. Geophys. Res.*, *112*, A11307, doi:10.1029/2007JA012383.
- Russell, J. M., III, M. G. Mlynczak, L. L. Gordley, J. Tansock, and R. Esplin (1999), An overview of the SABER experiment and preliminary calibration results, in *Optical Spectroscopic Techniques and Instrumentation for Atmospheric and Space Research III, Proc. SPIE Int. Soc. Opt. Eng.*, *3756*, 277–288.
- Sandanger, M., F. Søråas, K. Aarsnes, K. Oksavik, and D. S. Evans (2007), Loss of relativistic electrons: Evidence for pitch angle scattering by electromagnetic ion cyclotron waves excited by unstable ring current protons, *J. Geophys. Res.*, *112*, A12213, doi:10.1029/2006JA012138.
- Seppälä, A., M. A. Clilverd, and C. J. Rodger (2007a), NO_x enhancements in the middle atmosphere during 2003–2004 polar winter: Relative significance of solar proton events and the aurora as a source, *J. Geophys. Res.*, *112*, D23303, doi:10.1029/2006JD008326.
- Seppälä, A., P. T. Verronen, M. A. Clilverd, C. E. Randall, J. Tamminen, V. Sofieva, L. Backman, and E. Kyrölä (2007b), Arctic and Antarctic polar winter NO_x and energetic particle precipitation in 2002–2006, *Geophys. Res. Lett.*, *34*, L12810, doi:10.1029/2007GL029733.
- Shimazaki, T. (1984), *Minor Constituents in the Middle Atmosphere*, *Dev. Earth Planet. Phys.*, vol. 6, D. Reidel, Dordrecht, Netherlands.
- Siskind, D. E. (2000), On the coupling between the middle and upper atmospheric odd nitrogen, in *Atmospheric Science Across the Stratosphere*, *Geophys. Mongr. Ser.*, vol. 123, pp. 101–116, AGU, Washington, D. C.
- Solomon, S., P. J. Crutzen, and R. G. Roble (1982), Photochemical coupling between the thermosphere and the lower atmosphere: 1. Odd nitrogen from 50 to 120 km, *J. Geophys. Res.*, *87*, 7206–7220, doi:10.1029/JC087iC09p07206.
- Thomas, L., and M. R. Bowman (1986), A study of pre-sunrise changes in negative ions and electrons in the D-region, *Ann. Geophys.*, *4*, 219–228.
- Tobiska, W. K., T. Woods, F. Eparvier, R. Viereck, L. D. B. Floyd, G. Rottman, and O. R. White (2000), The SOLAR2000 empirical solar irradiance model and forecast tool, *J. Atmos. Terr. Phys.*, *62*, 1233–1250, doi:10.1016/S1364-6826(00)00070-5.
- Tsurutani, B. T., et al. (2006), Corotating solar wind streams and recurrent geomagnetic activity: A review, *J. Geophys. Res.*, *111*, A07S01, doi:10.1029/2005JA011273.
- Turunen, E., H. Matveinen, J. Tolvanen, and H. Ranta (1996), D-region ion chemistry model, in *STEP Handbook of Ionospheric Models*, edited by R. W. Schunk, pp. 1–25, Sci. Comm. on Sol. Terr. Phys. Secr., Boulder, Colo.
- Turunen, E., P. T. Verronen, A. Seppälä, C. J. Rodger, M. A. Clilverd, J. Tamminen, C.-F. Enell, and Th. Ulich (2009), Impact of different energies of precipitating particles on NO_x generation in the middle and upper atmosphere during geomagnetic storms, *J. Atmos. Sol. Terr. Phys.*, doi:10.1016/j.jastp.2008.07.005, in press.
- Verronen, P. T., E. Turunen, T. Ulich, and E. Kyrölä (2002), Modelling the effects of the October 1989 solar proton event on mesospheric odd nitrogen using a detailed ion and neutral chemistry model, *Ann. Geophys.*, *20*, 1967–1976.
- Verronen, P. T., A. Seppälä, M. A. Clilverd, C. J. Rodger, E. Kyrölä, C.-F. Enell, T. Ulich, and E. Turunen (2005), Diurnal variation of ozone depletion during the October–November 2003 solar proton events, *J. Geophys. Res.*, *110*, A09S32, doi:10.1029/2004JA010932.
- von Clarmann, T., N. Glatthor, M. Höpfner, S. Kellmann, R. Ruhnke, G. P. Stiller, H. Fischer, B. Funke, S. Gil-López, and M. López-Puertas (2005), Experimental evidence of perturbed odd hydrogen and chlorine chemistry after the October 2003 solar proton events, *J. Geophys. Res.*, *110*, A09S45, doi:10.1029/2005JA011053.

M. A. Clilverd, Physical Sciences Division, British Antarctic Survey, NERC, High Cross, Madingley Road, Cambridge CB3 0ET, UK. (macl@bas.ac.uk)

J. U. Kozyra, Department of Atmospheric, Oceanic and Space Sciences, College of Engineering, University of Michigan, 2455 Hayward, Ann Arbor, MI 48109-2143, USA. (jukozyra@umich.edu)

M. G. Mlynczak, NASA Langley Research Center, Hampton, VA 23681-0001, USA. (martin.g.mlynczak@nasa.gov)

C. J. Rodger, Department of Physics, University of Otago, P.O. Box 56, Dunedin, New Zealand. (crodger@physics.otago.ac.nz)

A. Seppälä, Finnish Meteorological Institute, P.O. Box 503, FIN-00101 Helsinki, Finland. (annika.seppala@fmi.fi)